JOURNAL OF THERMOPHYSICS AND HEAT TRANSFER
Vol. 24, No. 3, July–September 2010

Experimental Investigation of Mist Sprays Impinging on a Heated Cylinder

Roy J. Issa,* Emily M. Hunt,† and Freddie J. Davis‡
West Texas A&M University, Canyon, Texas 79016

DOI: 10.2514/1.42629

Experimental studies are conducted to investigate the effect of mist on the spray heat transfer in the cooling of a low-carbon steel cylindrical surface heated to the nucleate boiling temperature range. Multiple tests are performed to investigate the effect of the liquid mass flux, liquid-to-air loading, spray speed, and droplet size on the spray heat transfer along the circumference of the annulus cylinder. Infrared imaging is used to visualize the spray flow around the heated cylinder. Operating conditions for the air–mist spray cover variations in spray speed from 18 to 44 m/s, liquid mass flux from 0 to 1.54 kg/m^2 · s, and critical surface heat flux temperature from 123 to 130°C. The spray local heat transfer coefficients were obtained at various angular positions along the cylinder surface. The tests reveal that, with the introduction of a small amount of water in the spray, the heat transfer is dramatically increased. The spray heat transfer effectiveness decreases with the increase in the water mass flux. As a result, dilute sprays are more desirable than dense sprays in achieving higher heat transfer effectiveness and better efficiency for water utilization. The tests also reveal that, for the same spray speed and mean droplet flux, spray heat transfer effectiveness decreases with the increase in droplet size. The results of this study shall lead to a better understanding of the usage of dilute air–mist sprays in optimizing the cooling on a cylindrical surface.

Nomenclature

A_s = cylinder outer surface area, m^2
Bi = Biot number
c = low-carbon steel specific heat constant, J/kg · K
D_{noz} = nozzle exit diameter, m
D_o = cylinder outer diameter, m
d = median droplet diameter, μm
G = liquid mass flux, kg/m^2 · s
$\bar{h}_a$ = air surface average heat transfer coefficient, W/m^2 · K
h_{fg} = latent heat of vaporization, J/kg
h_s = spray (air and mist) heat transfer coefficient, W/m^2 · K
$\bar{h}_s$ = spray average heat transfer coefficient, W/m^2 · K
k_a = thermal conductivity of air, W/m · K
k_l = thermal conductivity of liquid water, W/m · K
m = cylinder mass, kg
N = mean droplet flux, 1/m^2 · s
Nu_s = spray Nusselt number
P_a = air pressure, psi
Pr_a = Prandtl number for air
q'' = heat flux, W/m^2
Re_{D_o} = Reynolds number for water flow over a cylinder
Re_l = Reynolds number for water flow at the nozzle exit
T = temperature, °C
T_s = surface temperature, °C
T_∞ = ambient (air) temperature, °C
t = time, s
V_s = spray velocity, m/s
ε = spray heat transfer effectiveness
μ_l = liquid water dynamic viscosity, Pa · s
ρ_l = liquid water density, kg/m

Presented as Paper 2008-3922 at the 40th AIAA Thermophysics Conference, Seattle, WA, 23–26 June 2008; received 8 December 2008; revision received 26 January 2010; accepted for publication 29 January 2010.

*Assistant Professor of Mechanical Engineering, Department of Engineering and Computer Science, Mechanical Engineering Division. Member AIAA.
†Assistant Professor of Mechanical Engineering, Department of Engineering and Computer Science, Mechanical Engineering Division.
‡Associate Professor and Head of Engineering and Computer Science Department.

I. Introduction

COOLING by air-assisted water sprays has been commercially used in many industrial applications because of the heat transfer benefits it has shown over conventional forced air. These applications include glass tempering, electronic chip cooling, and air–mist cooling of agricultural products. Several investigators have studied the heat transfer from a heated cylinder aligned normal to a flow stream of air and water droplets. Hodgson et al. [1] and Mednick and Colver [2] used large droplets with an average size of 360 and 1200 μm, respectively, in their air–water spray cooling of cylinders held at constant temperatures. Kosky [3] used steam (around 100°C) with air that is swept across a roughened heated tube, but there was no mention of the size of the water droplets used in the study. Basilico et al. [4] conducted tests on a cylinder heated to 40°C using air mist with a Sauter mean diameter of 9.25 μm, whereas Sabri et al. [5] conducted air–mist studies using droplets with an average size of 20 μm. Aihara et al. [6] used sprays that disperse droplets with an average Rosin–Rammler diameter ranging from 105 to 168 μm in the cooling of a cylinder heated to around 60°C. Trela and Mikielewicz [7] investigated the rivulet formation on a slightly heated cylinder (30–50°C) using air-assisted water sprays with droplets with a Sauter mean diameter of 80 μm. Han et al. [8] derived an analytical solution for the convective transport process in the flowfield around a cylinder. Allais et al. [9] conducted a study on the cooling of agricultural products by simulating the air–mist cooling of a cylindrical surface heated to temperatures less than 60°C using droplets with a Sauter mean diameter of 30 μm. Yoon et al. [10] conducted a study on the rebound and sticking of water droplets on a heated cylinder, but no heat transfer analysis was conducted. Recent experimental studies were conducted by Chen et al. [11,12] on a flat metallic surface to isolate the effect of droplet parameters such as droplet size, velocity, and mass flux on the spray critical heat flux and heat transfer effectiveness. Their results show that, to maximize the spray critical heat flux, it is desirable to use nozzles that produce very fine droplet sizes with high impinging velocities. However, very few researchers have conducted experimental studies on cylindrical surfaces for the heat transfer in the nucleate boiling region using sprays with various size droplets, water flow rates, and liquid-to-air loadings.

Droplets' impaction onto the target surface is strongly influenced by the liquid-to-air loading ratio in the spray. This is defined as the ratio of the water to air mass flow rate. The size of the water droplets produced by a nozzle dispersing air mist is controlled by the nozzle's air and water operating pressures. Small size droplets can be generated by either increasing the air pressure while decreasing the liquid pressure, or by increasing the air flow rate while decreasing the liquid flow rate. An increase in the pressure difference between the liquid and air streams results in an increase in the relative velocity between them. This leads to an increase in the shear force acting on the liquid film, and as a result, finer droplets can be generated. Increasing the air mass flow rate while keeping the water mass flow rate the same will result in an increase in the droplets' momentum, which will lead to an increase in the droplets' impaction efficiency on the target surface [13].

There is supporting evidence that shows the droplet size in the spray has a strong effect on the heat transfer enhancement [13–15]. Droplets impinging on the surface with a higher momentum result in better cooling due to the increase in the droplet spread on the surface. However, if the droplets are too large and the water flow flux is large enough, there is a risk that water flooding may occur on the surface. On the other hand, smaller size droplets have a better chance of evaporating on the surface if they make it to the surface. However, the impaction efficiency of small-size droplets is very low due to the increase in the number of droplets drifting away or evaporating before hitting the surface. Therefore, to maximize the droplets' impaction and heat transfer effectiveness, an optimal spray droplet size has to be employed. The selection of this optimal droplet size depends on the spray (water and air) flow operating conditions, ambient temperature, relative humidity, and the location of the nozzle with respect to the surface [13]. An increase in the nozzle-to-surface distance will result in a decrease in the droplet impaction velocity (and, therefore, in a decrease in the droplet incoming momentum) due to the longer time the drag force will be acting on the airborne droplet. An increase in the relative humidity will result in a decrease in the droplets' evaporation rate, and therefore, smaller droplets will have a better chance reaching the target surface.

The heat transfer associated with the spray cooling of a heated surface can be empirically evaluated using an effectiveness parameter. This parameter relates the amount of heat removed by the spray to the maximum possible heat transfer that can be achieved when the liquid droplets completely evaporate. The spray heat transfer effectiveness is expressed as

$$\varepsilon = \frac{q''}{Gh_{fg}} \tag{1}$$

Sprays using air and water are more efficient than those using water alone. This is because air injected with water increases the droplets momentum and enhances the impaction. The more the droplet spreads during impaction, the higher the spray heat transfer effectiveness is, due to the increase in the contact interface between the liquid droplet and the solid surface. For sufficiently high incoming droplet momentum, better droplet-to-surface contact and, therefore, better surface wetting can be established as long as surface flooding is minimized. Surface flooding is detrimental to the heat transfer effectiveness due to the increase in droplet-to-droplet interaction.

The objective of this research is to conduct experimental parametric studies to investigate the effect of the spray operating conditions on the heat transfer enhancement in the cooling of a cylindrical surface heated to temperatures in the nucleate boiling region. Besides the spray droplet size, test measurements will show the dependency of the air–water spray heat flux and heat transfer effectiveness on other factors, such as the liquid-to-air loading, liquid flow flux, and spray speed.

II. Experimental Setup

Figure 1 shows the overall experimental system setup. The water used in the conducted tests has been treated by reverse-osmosis

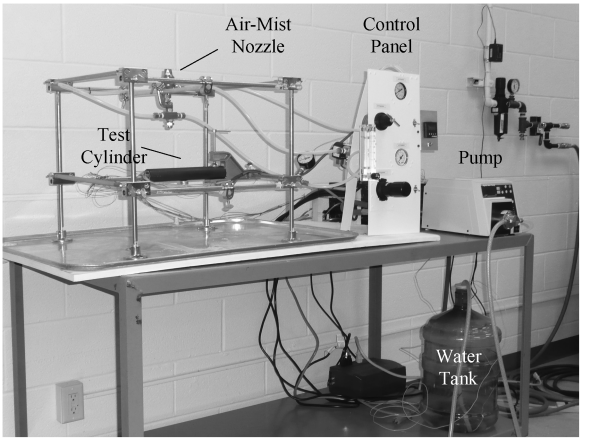

Fig. 1 Overall experimental system setup.

cleaning. A digital gear pump by Cole–Parmer (micropump gear model no. 75211) increases the water pressure to a level necessary for spraying. The gear pump provides a continuous water flow rate that ranges from 15 to 940 mL/min. The water is controlled and regulated by a three-way solenoid valve (controlled by an electrical switch) and a regulator. The three-way solenoid valve has air running through it. Once the solenoid is actuated, it allows air to reach the upper inlet of the nozzle and opens the valve for water to flow through. Air at a 120 psi maximum pressure is provided to the lab by an air supply line from a compressor placed outside the lab building. The air pressure is regulated before entering the nozzle air chamber, and air is controlled by a two-way solenoid valve that is activated by an electrical switch. Flow and pressure gauges are installed on the air and water pipe lines.

The nozzle system consists of an air-actuated nozzle body assembly (Spraying Systems, Inc. part no. 10535-1/4J) and a spray setup fixture consisting of air and fluid caps (Spraying Systems, Inc. part no. SU11). The orifice diameter of the nozzle exit is about 1 mm. This particular nozzle provides a spectrum of droplet sizes ranging from 5 to 100 μ. The size of the water droplets produced is controlled by the nozzle operating flow conditions and the liquid-to-air loading ratio. Smaller-size droplets can be generated by increasing the air pressure while decreasing the liquid pressure and vice versa.

The test section consists of a low-carbon steel annulus cylinder, situated at a distance of 10 cm below the nozzle. The cylinder outer diameter is 38 mm and the inner diameter is 28 mm. Eight holes (2 mm in diameter and 76 mm deep) are drilled into the cylinder wall. Figure 2 shows a close-up view of the location of the drilled holes along the cylinder wall. The cylinder is heat treated to minimize oxidation from the water in the spray. A cartridge heater (around 64 mm in length) is installed inside the cylinder. Eight thermocouples of type K are imbedded inside the drilled holes to record the temperature variation during the air–mist surface quenching. An additional thermocouple is cemented onto the cartridge heater

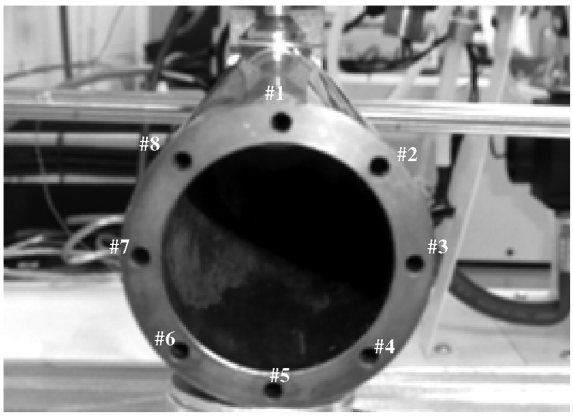

Fig. 2 Arrangement of the drilled holes on the test cylinder.

Table 1 Test cases operating conditions

Case	P_{air}, psi (MPa)	P_{water}, psi (MPa)	Vs, m/s	Water flow rate, gph (m^3/s)	Liquid-to-air Loading	Median droplet diameter, μm
1	5 (0.034)	——	18.3	0	——	——
2	5 (0.034)	3 (0.021)	18.3	0.25 (2.6×10^{-7})	15.8	44
3	5 (0.034)	9 (0.062)	18.3	0.5 (5.3×10^{-7})	31.6	60
4	5 (0.034)	11 (0.076)	18.3	1.0 (1.1×10^{-6})	63.0	70
5	5 (0.034)	14 (0.097)	18.3	1.5 (1.6×10^{-6})	94.8	85
6	10 (0.069)	——	24.7	0	——	——
7	10 (0.069)	10 (0.069)	24.7	0.5 (5.3×10^{-7})	23.3	53
8	10 (0.069)	14 (0.097)	24.7	1.0 (1.1×10^{-6})	46.6	63
9	10 (0.069)	16.5 (0.114)	24.7	1.5 (1.6×10^{-6})	70.1	77
10	30 (0.207)	——	43.6	0	——	——
11	30 (0.207)	24 (0.165)	43.6	1.0 (1.1×10^{-6})	26.4	42
12	30 (0.207)	29 (0.200)	43.6	1.5 (1.6×10^{-6})	39.7	53
13	30 (0.207)	33 (0.228)	43.6	2.0 (2.1×10^{-6})	52.8	65

surface to control the temperature setting of the heater. Two more thermocouples are also used to record the incoming air and water temperatures. All thermocouple wires are connected to a data-acquisition device (Omega OMB-CHARTSCAN-1400), which in turn is connected to a portable computer that records the temperature data on the hard disk drive at a sampling rate of 1 data point per second. Table 1 shows the test cases conducted in this study. Table A1 shows the uncertainties in the experimental data.

An infrared camera (FLIR Systems, Inc., ThermoVision A40) was used to take thermal images of the air–mist spray around the heated cylinder, and some of the test cases are presented in this study. The colors in the infrared images are not intended for temperature evaluation, but only to visualize the spray flow around the cylinder. The air–mist spray is shown in black, in contrast to the heated cylinder that is shown in white. Figure 3 corresponds to test case 3, in which the spray speed is 18.3 m/s, the water flow rate is 0.5 gph, and the droplet size is 60 μm. With this dilute spray, the infrared image shows the air–mist spray impinging at the forward part of the cylinder surface, while the rear part remains unwetted. During the test, vapor was seen to be generated from the droplets impaction. Figure 4 corresponds to test case 13, in which the spray speed is 43.6 m/s, the water flow rate is 2 gph, and the droplet size is 65 μm. This is a much denser spray, and the thermal image shows more water engulfing the cylinder at the forward and at the rear part as well. The incoming spray and the generated vapor is shown to be pushed downstream by the incoming air–mist flow. The spray angle at the nozzle exit is also shown to increase with the increase in the water flow rate.

III. Results and Discussions

A. Heat Transfer Test Measurements

The air velocity at the nozzle exit is measured using a high-speed anemometer. The spray velocity is shown to increase from 18.3 to 43.6 m/s as the air pressure increases from 5 to 30 psi (Fig. 5). In this study, a full conical spray is injected onto the outer surface of the 38 mm low-carbon steel cylinder shown in Fig. 2. For the test cases that are conducted, the nozzle spray exit angle is around 13 deg. Tests conducted by the nozzle manufacturer (Spraying Systems, Inc.) show the spray angle to increase slightly by few degrees with the substantial increase in either the liquid or air flow rates. Figure 6 shows the effect of the nozzle flow operating conditions on the median droplet diameter in the spray tests. This data is adapted from studies conducted on this type of nozzle at the Spraying Systems, Inc. research facility [16].

To minimize the effect of surface oxidation, the test cylinder is cleaned with emery paper and liquid cleaner before each test case to remove any oxide depositions that buildup on the surface. In all test cases, the cylinder surface is heated to the critical heat flux

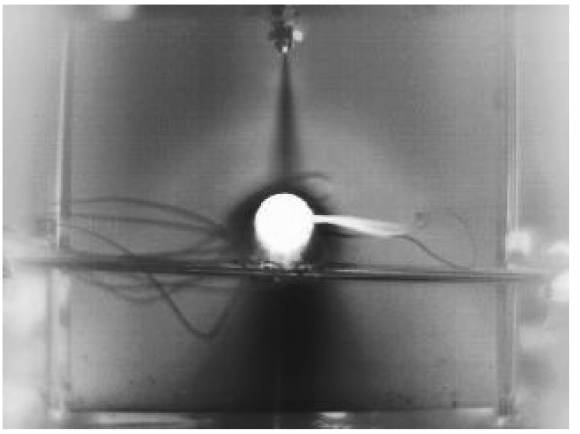

Fig. 4 Infrared image of the spray flow (test case 13).

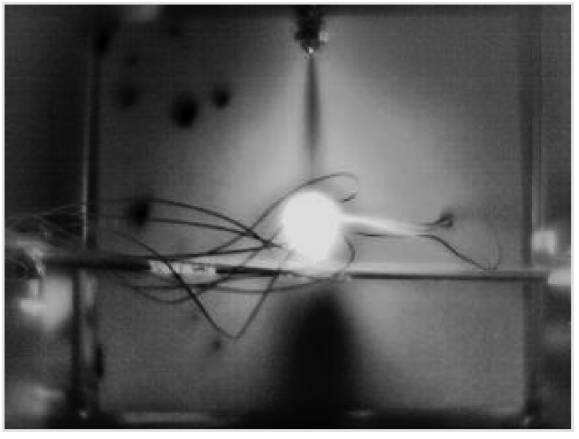

Fig. 3 Infrared image of the spray flow (test case 3).

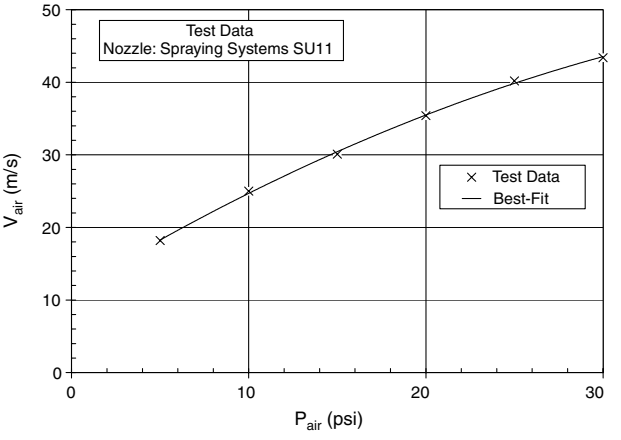

Fig. 5 Air velocity test measurements.

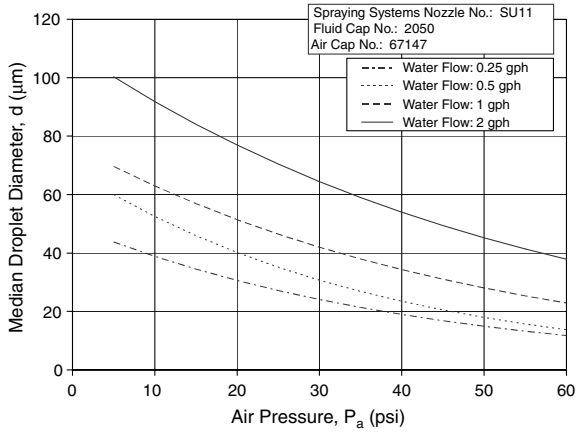

Fig. 6 Spray characteristics for SU11 nozzle (data adapted from [16]).

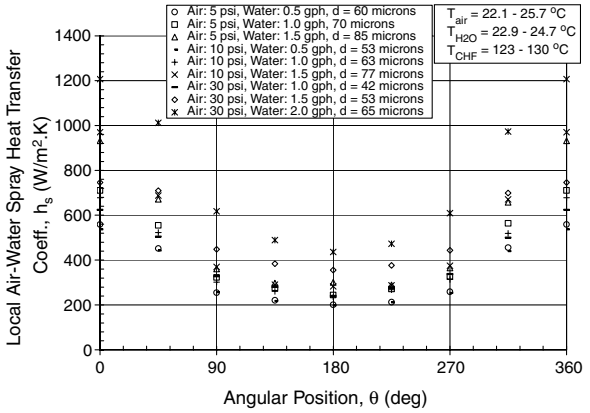

Fig. 7 Local spray heat transfer coefficient versus angular position on the cylinder.

temperature ranging from 123 to 130°C. Thermocouples of type K are imbedded inside the eight holes drilled along the cylinder wall. The thermocouple wires are insulated using glass braid material to withstand the high temperatures. The temperature time history of the thermocouples is recorded using a digital data-acquisition system. At the beginning of each test case, the cartridge heater is turned on, and after a steady-state temperature is reached at the outer surface, the air–mist nozzle is turned on. Air and water flow rates are turned off once the cylinder surface reaches a steady-state temperature again.

The annulus cylinder is made of low-carbon steel material, which has a high thermal conductivity. Because of that, and for the amount of water mass flow rates used, the Biot number associated with the air–mist spray is less than 0.1 in all the conducted cases. Therefore, it is reasonable to assume the lumped capacitance method to be valid in the evaluation of the air–mist heat transfer coefficient, and the inverse conduction method is not necessary:

$$mc\frac{\mathrm{d}T}{\mathrm{d}t} = h_s A_s (T_s - T_\infty) \tag{2}$$

Test results for the cases in which air alone is flowing over the cylinder compares well (within 5% error) with the empirical correlation given by Hilpert [17] for the air heat transfer coefficient:

$$\bar{h}_a = 0.027\frac{k_a}{D_o} Re_{D_o}^{0.805} Pr_{D_o}^{0.805} \tag{3}$$

The local air–mist heat transfer coefficient is calculated for the eight angular positions on the cylinder surface and the results are shown in Table 2. For certain flow conditions (such as cases 2 and 3), a negligible amount of water spray is seen during the test to hit the surface at thermocouple location 5, whereas for other flow conditions (such as cases 12 and 13), water is seen to engulf almost the complete cylinder perimeter. In all cases, the heat transfer coefficient associated with location 5, which is at 180 deg with respect to location 1, has the lowest measurable value. There is a slight offset in the calculation of the spray heat transfer coefficient between hole locations that are symmetrical to each other due to the slight error in drilling the holes and in the positioning of the thermocouples into the holes.

In Fig. 7, a comparison is made between the test cases in which air and water are both being dispersed. The test results show the heat transfer coefficient to be highest at the stagnation point; it gradually decreases as the hydrodynamic boundary layer develops over the cylinder surface. Quantitatively, the heat transfer coefficients (shown in Table 2) improve dramatically with the presence of mist. For example, at a 24.7 m/s spray velocity, the introduction of 1 gph (0.77 $\mathrm{kg/m^2 \cdot s}$) will increase the heat transfer coefficient by a factor of more than 4 at the stagnation point on the cylinder surface (directly below the nozzle exit) compared to cooling by air alone.

An average spray Nusselt number, $\bar{N}u_s$, over the cylindrical surface is calculated from the arithmetic average of the eight local heat transfer coefficient values along the circumference. The following empirical correlation is obtained between the spray Nusselt, $\bar{N}u_s$, and Reynolds numbers for water, Re_l:

$$\bar{N}u_s = 0.0109 Re_l + 7.53 \tag{4}$$

where

$$\bar{N}u_s = \bar{h}_s D_o / k_l \tag{5}$$

and

$$Re_l = \rho_l V_s D_{\mathrm{noz}} / \mu_l \tag{6}$$

The characteristic length used in the definition of the Reynolds number is taken to be the nozzle exit diameter, D_{noz}, whereas the characteristic length used in the definition of the Nusselt number is taken to be the cylinder outer diameter, D_o. Test data for the spray average Nusselt number versus Reynolds number for water are

Table 2 Experimental results for the spray heat transfer coefficient at various angular positions

Case	h_1, $\mathrm{W/m^2 \cdot k}$	h_2, $\mathrm{W/m^2 \cdot k}$	h_3, $\mathrm{W/m^2 \cdot k}$	h_4, $\mathrm{W/m^2 \cdot k}$	h_5, $\mathrm{W/m^2 \cdot k}$	h_6, $\mathrm{W/m^2 \cdot k}$	h_7, $\mathrm{W/m^2 \cdot k}$	h_8, $\mathrm{W/m^2 \cdot k}$
1	109	104	97	92	89	94	99	105
2	300	187	132	106	89	95	119	161
3	559	452	255	221	201	213	259	456
4	711	555	323	277	244	271	328	564
5	932	672	361	297	301	289	365	658
6	118	106	99	93	90	95	101	108
7	537	443	257	218	198	211	254	440
8	678	523	302	261	235	268	314	519
9	970	688	370	291	283	288	375	671
10	151	141	132	124	120	125	134	142
11	624	505	328	281	240	275	337	500
12	746	710	448	384	356	377	444	699
13	1207	1012	618	489	436	473	610	973

shown in Fig. 8. It is observed that the spray average Nusselt number increases almost linearly with the water Reynolds number. This is attributed to the fact that, for the low water mass flow fluxes of the experiments, the spray behaves close to an ideal spray.

Figure 9 shows the spray average heat transfer coefficient versus liquid-to-air loading. Experimental results are shown for spray speeds of 18.3, 24.7, and 43.6 m/s. The increase in the heat transfer coefficient at high liquid loadings and spray speeds is due to the ballistic impaction of the air–mist spray causing a tremendous increase in the number of satellite droplets generated during impaction at the surface. This has a favorable effect on enhancing the surface heat transfer because it is much easier for satellite droplets to evaporate and cool the thermal boundary layer on the surface. The results in Fig. 9 also show that, as the spray speed increases from 18.3 to 43.6 m/s, the spray heat transfer coefficient considerably increases. Droplets with higher impinging velocities tend to spread more at the surface. The more the droplets spread at the surface, the higher the heat transfer is.

Data gathered from the performed tests are further analyzed. The calculated spray liquid flow flux, G, spray critical heat flux, CHF, spray heat transfer effectiveness, ε, and mean droplet flux, N, are presented in Table 3. The relation between G and N is based on the following:

$$G = \rho_l \frac{\pi d^3}{6} N \tag{7}$$

B. Effect of Liquid Flux and Spray Speed on Heat Flux

The most conventional way to show the expected behavior of the spray is to plot the spray heat flux against the liquid mass flux. This is because the liquid mass flux has the strongest influence on the spray heat transfer. Figure 10 shows the spray critical heat flux at the stagnation point as function of the liquid mass flux for a spray speed that is varied by a factor of 2.4, a median droplet size that is varied by a factor of 2, and a fairly constant droplet temperature. The data

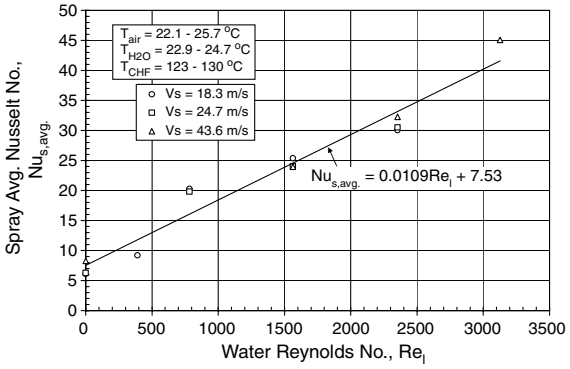

Fig. 8 Spray average Nusselt number versus water Reynolds number.

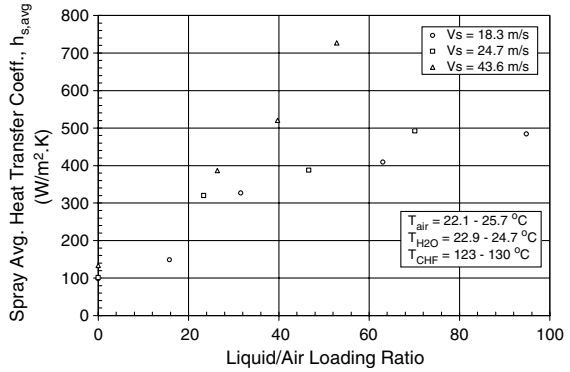

Fig. 9 Spray average heat transfer coefficient versus liquid-to-air loading ratio.

Table 3 Variation in G, CHF, ε, and N for the performed tests

Case	G, kg/m^2 · s	CHF, W/m^2	ε	N, 1/m^2 · s
1	0	1.12×10^4	——	——
2	0.19	3.23×10^4	7.4	4.39×10^9
3	0.39	5.76×10^4	6.6	3.42×10^9
4	0.77	7.33×10^4	4.2	4.37×10^9
5	1.16	9.85×10^4	3.8	3.61×10^9
6	0	1.24×10^4	——	——
7	0.39	5.65×10^4	6.5	4.96×10^9
8	0.77	7.25×10^4	4.2	5.92×10^9
9	1.16	1.01×10^5	3.9	4.86×10^9
10	0	1.48×10^4	——	——
11	0.77	6.42×10^4	3.7	1.99×10^{10}
12	1.16	7.87×10^4	3.0	1.49×10^{10}
13	1.54	1.23×10^5	3.5	1.07×10^{10}

indicate that the heat flux strongly increases with the liquid mass flux. The spray behaves almost like an ideal spray, for which the increase in the spray heat flux with respect to the liquid mass flux is close to linear. This is because, for the conducted tests, the liquid mass flux was less than 2 kg/m^2 · s, and dilute spray conditions prevailed. This effect was noted by Deb and Yao [18], who recommended the cutoff of 2 kg/m^2 · s for surface flooding.

Figure 11 shows the effect of the variation in the spray speed on the spray critical heat flux at the stagnation point. Experimental results are shown for two cases in which the spray median droplet diameter, d, is maintained at approximately 50 μm $\pm$ 10% and also at 70 μm $\pm$ 13%. For these cases, the corresponding mean droplet flux, N, is more relaxed at 8.1×10^9 1/m^2 · s $\pm$ 73% and 6.34×10^9 1/m^2 · s $\pm$ 61%, respectively. Holding the droplet diameter almost constant, the critical heat flux is shown to increase by almost a factor of 2 as the spray speed increases from 18.2 to 43.4 m/s. It is also noticed that decreasing the droplet size from 70 to 50 μm resulted in an increase in the spray heat flux by at least a factor of 1.5. This inverse relationship between the droplet diameter and spray heat flux has also been noted by Chen et al. [11,12] in their water spray cooling of a flat metallic surface.

C. Effect of Liquid Flux and Droplet Diameter on Spray Effectiveness

The variation in the spray heat transfer effectiveness with the liquid mass flux is shown in Fig. 12. The results are shown for the performed test cases for spray droplets ranging from 42 to 85 μm, spray velocities ranging from 18.2 to 43.4 m/s, and critical heat fluxes ranging from 123 to 130°C. The results show the spray heat transfer effectiveness to decrease as the liquid mass flux increases due to the interaction that occurs between the droplets. As the liquid mass flux increases, previous spray droplets do not have sufficient time to get out of the way of newly incoming droplets. These newly incoming droplets will impact any liquid water film existing on the surface first, which decreases their momentum and increases their temperature by mixing with the already warmer liquid on the surface.

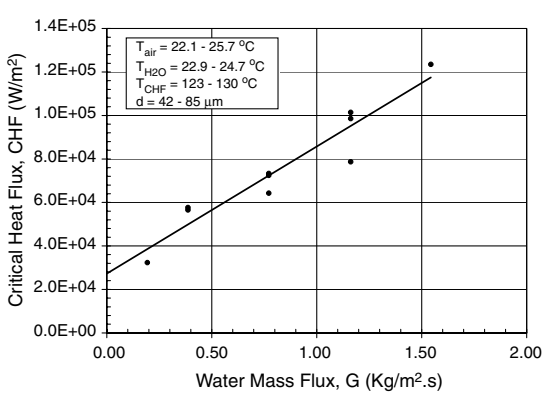

Fig. 10 Critical heat flux versus water mass flux at the stagnation point.

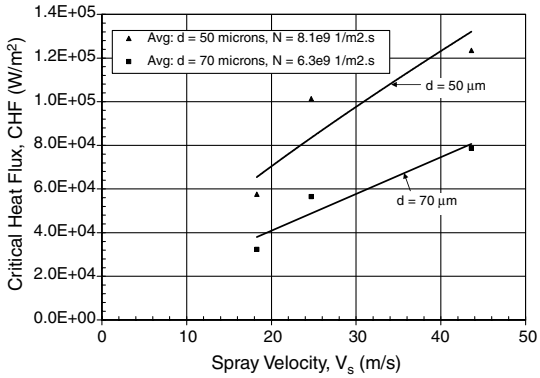

Fig. 11 Critical heat flux versus spray velocity at the stagnation point.

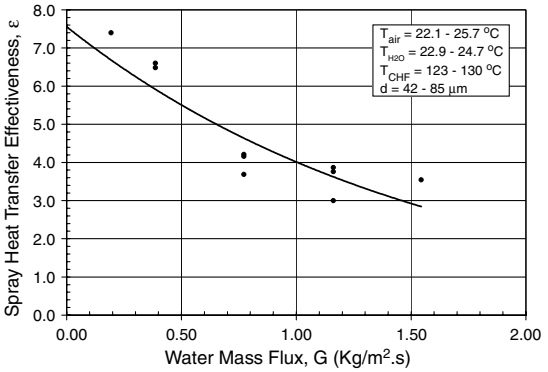

Fig. 12 Spray heat transfer effectiveness versus water mass flux.

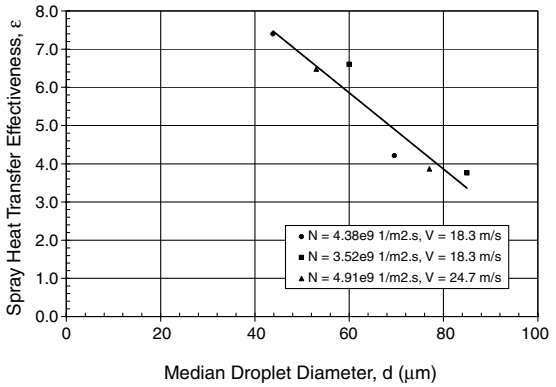

Fig. 13 Spray heat transfer effectiveness versus median droplet diameter.

As a result, the spray will then begin to lose its heat transfer effectiveness.

Figure 13 shows the relation between the spray heat transfer effectiveness and the spray droplet diameter for a fairly constant spray speed and mean droplet flux. Results are shown for three conditions: 1) a spray speed of 18.3 m/s with a corresponding mean droplet flux of 4.38×10^9 $1/m^2 \cdot s \pm 0.35\%$, 2) a spray speed of 18.3 m/s with a corresponding mean droplet flux of 3.52×10^9 $1/m^2 \cdot s \pm 3.9\%$, and 3) a spray speed of 24.7 m/s with a corresponding mean droplet flux of 4.91×10^9 $1/m^2 \cdot s \pm 1.5\%$. The results show a decrease in the spray heat transfer effectiveness with an increase in the droplet diameter. This is in agreement with the predictions of Chen et al. [11], who also reported that smaller droplets have higher cooling effectiveness than larger droplets.

IV. Conclusions

Experimental studies were conducted for the air–mist spray cooling of a low-carbon steel annulus cylinder heated to temperatures in the nucleate boiling range. Experiments were conducted to investigate the air–mist cooling of the heated cylinder at atmospheric pressure. Multiple tests were performed to investigate the effect of the liquid mass flux, liquid-to-air loading, spray speed, and droplet size on the surface heat transfer. An infrared camera was used to visualize the spray flow over the cylinder. The major conclusions of this study are as follows:

1) Heat transfer coefficient and heat flux are dramatically increased with the introduction of mist with air.

2) The spray heat transfer coefficient increases with both the spray speed and the liquid mass flux.

3) Spray heat transfer effectiveness decreases with the increase in the water mass flux. Dilute sprays are more desirable for achieving higher heat transfer effectiveness and, therefore, result in better efficiency of liquid use.

4) The critical heat flux increases with spray speed while holding the spray droplet size and mean droplet flux within a narrow range.

5) For the same spray speed and mean droplet flux, the spray heat transfer effectiveness decreases with the increase in droplet diameter.

6) Wetting of the back surface of the cylinder increases with the increase in the liquid mass flux.

Appendix A: Uncertainties in the Experimental Data

Table A1 Uncertainties in the experimental data

Variables	Uncertainty
Measured variables	
Temperatures (K-type thermocouples)	±1.1°C
Air pressure	±3%
Water pressure	±3%
Air flow rate	±3%
Water flow rate	±0.3%
Dimensions	±0.03 mm
Properties	Negligible
Calculated variables	
Air–mist heat transfer coefficient	±9%

References

[1] Hodgson, J. W., Satebac, R. T., and Sunderland, J. E., "An Experimental Investigation of Heat Transfer from a Spray Cooled Isothermal Cylinder," *Journal of Heat Transfer*, Vol. 90, No. 4, 1968, pp. 457–463.

[2] Mednick, R. L., and Colver, C. P., "Heat Transfer from a Cylinder in an Air–Water Flow Stream," *American Institute of Chemical Engineers Journal*, Vol. 15, No. 3, 1969, pp. 357–361. doi:10.1002/aic.690150311

[3] Kosky, P. G., "Heat Transfer to Saturated Mist Flowing Normally to a Heated Cylinder," *International Journal of Heat and Mass Transfer*, Vol. 19, No. 5, 1976, pp. 539–543. doi:10.1016/0017-9310(76)90167-8

[4] Basilico, C., Jung, G., and Martin, M., "Etude du Transfert Convectif Entre un Cylindre Chauffe et un Ecoulement d'Air Charge de Gouttelettes d'Eau," *International Journal of Heat and Mass Transfer*, Vol. 24, No. 3, 1981, pp. 371–385. doi:10.1016/0017-9310(81)90045-4

[5] Sabri, M., Basilico, C., and Martin, M., "Etude des Structures Convectives et du Transfert Thermique Autour d'un Cylindre en Deuxieme Nappe dans une Configuration en Quinconce, en Ecoulement d'Air Chargé de Gouttelettes d'Eau," *International Journal of Heat and Mass Transfer*, Vol. 30, No. 9, 1987, pp. 1859–1870. doi:10.1016/0017-9310(87)90245-6

[6] Aihara, T., Fu, W. S., Hongoh, M., and Shimoyama, T., "Experimental Study of Heat and Mass Transfer from a Horizontal Cylinder in Downward Air–Water Mist Flow with Blockage Effect," *Experimental Thermal and Fluid Science*, Vol. 3, No. 6, 1990, pp. 623–631. doi:10.1016/0894-1777(90)90079-M

[7] Trela, M., and Mikielewicz, J., "An Analysis of Rivulet Formation during Flow of an Air/Water Mist Across a Heated Cylinder," *International Journal of Heat and Mass Transfer*, Vol. 35, No. 10, 1992, pp. 2429–2434. doi:10.1016/0017-9310(92)90085-7

[8] Han, R. J., Moss, O. R., and Wong, B. A., "Derivation and Application of an Analytical Solution of the Mass Transfer Equation to the Case of Forced Convective Flow Around a Cylindrical and a Spherical Particle with Fluid Surface Properties," *Journal of Aerosol Science*, Vol. 27, No. 2, 1996, pp. 235–247. doi:10.1016/0021-8502(95)00548-X

[9] Allais, I., Alvarez, G., and Flick, D., "Analyse du Transfert Thermique Entre un Cylinder et un Ecoulement d'Air Faiblement Chargé en Gouttelettes d'Eau," *International Journal of Thermal Sciences*, Vol. 36, No. 4, 1997, pp. 276–288. doi:10.1016/S0035-3159(97)80688-5

[10] Yoon, S. S., Des Jardin, P. E., Presser, C., Hewson, J. C., and Avedisian, C. T., "Numerical Modeling and Experimental Measurements of Water Spray Impact and Transport over a Cylinder," *International Journal of Multiphase Flow*, Vol. 32, No. 1, 2006, pp. 132–157. doi:10.1016/j.ijmultiphaseflow.2005.05.007

[11] Chen, R. H., Chow, L. C., and Navedo, J. E., "Optimal Spray Characteristics in Water Spray Cooling," *International Journal of Heat and Mass Transfer*, Vol. 47, 2004, pp. 5095–5099. doi:10.1016/j.ijheatmasstransfer.2004.05.033

[12] Chen, R. H., Chow, L. C., and Navedo, J. E., "Effects of Spray Characteristics on Critical Heat Flux in Subcooled Water Spray Cooling," *International Journal of Heat and Mass Transfer*, Vol. 45, 2002, pp. 4033–4043. doi:10.1016/S0017-9310(02)00113-8

[13] Issa, R., "Optimal Spray Characteristics in the Air-Assisted Water Spray Cooling of a Downward-Facing Heated Surface," *Proceedings of the 24th ASM International Heat Treating Society Conference*, Detroit, Michigan, 2007.

[14] Issa, R., and Yao, S. C., "Numerical Model for Spray-Wall Impactions and Heat Transfer at Atmospheric Conditions," *Journal of Thermophysics and Heat Transfer*, Vol. 19, No. 4, 2005, pp. 441–447. doi:10.2514/1.11200

[15] Issa, R., and Yao, S. C., "A Numerical Model of the Mist Dynamics and Heat Transfer at Various Ambient Pressures," *Journal of Fluids Engineering*, Vol. 127, No. 4, 2005, pp. 631–639. doi:10.1115/1.1976743

[16] Schick, R. J., and Knasiak, K. F., "Characterization of Two Fluid Spray Nozzles for NOx Control Applications," Spraying Systems, Inc, Rept. 002, Wheaton, IL, 2003.

[17] Hilpert, R., "Warmeabgabe von Geheizten Drahten ond Rohren in Luftstrom," *Forschung auf dem Gebiete des Ingenieurwesens*, Vol. 4, 1933, pp. 215–224. doi:10.1007/BF02719754

[18] Deb, S., and Yao, S. C., "Analysis on Film Boiling Heat Transfer of Impacting Sprays," *International Journal of Heat and Mass Transfer*, Vol. 32, No. 11, 1989, pp. 2099–2112. doi:10.1016/0017-9310(89)90117-8